Electroweak effects in $e^+e^- \to e^+e^-$ at $\sqrt{s} = 29$ GeV

E. Fernandez,* W. T. Ford, N. Qi, A. L. Read, Jr., and J. G. Smith
Department of Physics, University of Colorado, Boulder, Colorado 80309

T. Camporesi,† I. Peruzzi, and M. Piccolo
Istituto Nazionale di Física Nucleare, Laboratori Nazionali di Frascati, Frascati, Italy

H. T. Blume, R. B. Hurst, K. H. Lau, J. Pyrlik, J. P. Venuti,
H. B. Wald, and Roy Weinstein
Department of Physics, University of Houston, Houston, Texas 77004

H. R. Band, M. W. Gettner, G. P. Goderre, J. H. Moromisato, W. D. Shambroom,‡
J. C. Sleeman, and E. von Goeler
Department of Physics, Northeastern University, Boston, Massachusetts 02115

W. W. Ash, G. B. Chadwick, R. E. Leedy, R. L. Messner, L. J. Moss, F. Muller,§
H. N. Nelson, D. M. Ritson, L. J. Rosenberg, D. E. Wiser, and R. W. Zdarko
Department of Physics and Stanford Linear Accelerator Center, Stanford University, Stanford, California 94305

D. E. Groom and P. G. Verdini
Department of Physics, University of Utah, Salt Lake City, Utah 84112

M. C. Delfino, B. K. Heltsley,** J. R. Johnson, T. L. Lavine, T. Maruyama, and R. Prepost
Department of Physics, University of Wisconsin, Madison, Wisconsin 53706

(Received 23 June 1986)

A high-precision measurement of the differential cross section for Bhabha scattering ($e^+e^- \to e^+e^-$) is presented. The measurement was performed with the MAC detector at the PEP storage ring of the Stanford Linear Accelerator Center, at a center-of-mass energy of 29 GeV. Effects due to electroweak interference are observed and agree well with the predictions of the Glashow-Salam-Weinberg model. The agreement between the data and the electroweak prediction rules out substructure of the electron up to mass scales of 1 TeV.

I. INTRODUCTION

This paper presents results from a high-precision measurement of the differential cross section for Bhabha scattering ($e^+e^- \to e^+e^-$), at a center-of-mass energy ($E_{\text{c.m.}}$) of 29 GeV, from the MAC detector operating at the SLAC storage ring PEP. Bhabha scattering is a fundamental process which can be calculated within the framework of electroweak theory,[1] and precision measurements can therefore be used to test the theory and determine its parameters. Bhabha scattering is also widely used in e^+e^- physics as a luminosity monitor, giving added importance to a complete understanding of this process.

The interference between the vector and axial-vector components of the electroweak current leads to the well-known charge asymmetry in $e^+e^- \to \mu^+\mu^-$ (Ref. 2), the study of which has provided high-precision measurements of the product of the electron and muon electroweak theory axial-vector couplings ($g_A^e g_A^\mu$). The electroweak interaction also leads to a modification of the total cross section for muon pair production which could, in principle, be used to determine a value for the product of electroweak vector couplings $g_V^e g_V^\mu$. Unfortunately, this modification is too small to be measured to a useful precision due to experimental systematic errors involved in measuring the total cross section.

The situation is different in electroweak Bhabha scattering.[3] The QED spacelike diagram dominates and gives the $e^+e^- \to e^+e^-$ cross section a charge asymmetry of essentially 100%, totally obscuring any weak asymmetry effects. However, the presence of the weak diagrams leads to a modification of the cross section as a function of momentum transfer squared (q^2), resulting in a maximum deviation from pure QED of about 2% for favored values of the coupling constants. It should be noted that the vector and axial-vector couplings modify the Bhabha differential cross section in a similar manner; this is in sharp contrast to the $\mu^+\mu^-$ case noted above. Furthermore, since the final state is the same as the initial state, it is possible to extract the actual coupling constants for the electron, rather than the product of the electron and muon couplings. Finally, a comparison of results from $\bar{\nu}_e e^-$ scattering with the present measurement allows the sign of the couplings to be determined.

As the electroweak effects are small, it is essential to

understand the systematic errors. This analysis used data collected over a contiguous, high luminosity run at PEP with no changes in the configuration of the machine or detector hardware. The large uncertainties introduced by charge misidentification in the MAC detector, especially at small scattering angles, made it necessary to measure the angular distribution without attempting to identify the charge of the particles, resulting in some loss of sensitivity. In the following, $|\cos\theta|$ refers to the absolute value of the cosine of the polar angle[4] and the measured cross section is

$$\frac{d\sigma}{d\Omega}(|\cos\theta|)=\frac{d\sigma}{d\Omega}(\cos\theta)+\frac{d\sigma}{d\Omega}(-\cos\theta)\ .$$

II. THE MAC DETECTOR

The MAC detector has been described in detail elsewhere.[5] The elements which are essential to this analysis are the central drift chamber (CD), the electromagnetic shower calorimeter (SC), and the trigger hardware. A brief overview of the detector, as well as a more detailed description of the SC, are given in the preceding paper on $e^+e^- \to \gamma\gamma$ (Ref. 6).

The cylindrical drift chamber (CD) consists of 833 drift cells arranged in 10 concentric cylindrical layers inside a common gas volume filled with a 90% Ar–10% CH_4 mixture. Each cell consists of two closely spaced sense wires, held together by small epoxy beads, centered in an electrostatic cage created by 12 field wires and connected to discriminators followed by time-to-digital converters (TDC's). The use of a double sense wire resolves the left-right ambiguity in hardware, simplifying the track-reconstruction software. Six of the layers are tilted with respect to the beam axis in order to allow measurement of the z position of the track crossing with stereoscopic techniques. The drift chamber is surrounded by a solenoid coil with a central magnetic field of 0.57 T, providing momentum analysis as well as tracking of charged particles. Representative resolutions are $\sigma(1/p)=0.065\sin\theta$ $(\mathrm{GeV}/c)^{-1}$, $\sigma(\phi)=0.2°$, and $\sigma(\theta)=0.7°$, where p is the momentum of the particle, θ is the polar angle measured with respect to the direction of the incoming positron beam, and ϕ is the azimuthal angle.

Segmented scintillation counters are imbedded in the hadron calorimeter surrounding the SC, in the form of a hexagonal prism, to provide trigger and time-of-flight information. Each sextant of the central section has a plane formed from 12 counters and each end cap has a hexagonal wall formed from 36 counters. The individual phototube signals are split to feed an analog-to-digital converter (ADC), a TDC, and a discriminator for each counter. The thresholds on the discriminators are adjusted such that they detect minimum ionizing particles with nearly 100% efficiency.

Bhabha events were obtained from two orthogonal triggers.

(a) The scintillator trigger uses signals from the scintillation counter discriminators and the CD cell discriminators. Logical *OR* combinations of the individual scintillator discriminators are used to form signals corresponding to four azimuthal quadrants in each end cap and six sextants in the central section. A coincidence of opposite quadrants or sextants is required. The trigger is further refined by requiring a rough azimuthal coincidence between the scintillators causing the pattern above and at least three CD cell discriminators.

(b) The energy trigger uses signals from partial energy sums provided by the preamplifiers in the proportional-wire-chamber system, which are summed further to form nine signals: six sextants of SC, one total sum of the central hadron calorimeter and one sum each for the two end-cap calorimeters. These sums are fed into timing energy discriminators[7] with typical thresholds of 3 GeV. In order to reduce noise effects, the central hadron and end-cap calorimeter energy sums are required to be in coincidence with the logical OR of all scintillator counter signals in the appropriate region of the detector.

III. CANDIDATE-EVENT SELECTION

Ideally, events from Bhabha scattering would have two distinct signatures: two oppositely directed charged tracks in the CD that emerge from the beam interaction volume and energy deposition of approximately $E_{\mathrm{c.m.}}$ in the electromagnetic shower calorimeters.

In the real detector, less restrictive requirements must be made in order to account for resolution, beam noise, and electronic cross-talk effects. After extensive visual scanning of Bhabha-event candidates, the following criteria were used to define a two-prong event: (1) two CD tracks, only one of which is fitted as emerging from the interaction point (IP); or (2) two CD tracks, both fitted as emerging from the IP; or (3) three CD tracks, two of which emerge from the IP and the third one has fewer than five (out of a maximum possible of ten) drift cells in the track fit; or (4) three CD tracks, two of which emerge from the IP and the third one has momentum less than 500 MeV; or (5) three CD tracks, all emerging from the IP, where any two tracks are very close together ($|\Delta\phi|<5°$).

Case (2) represents the ideal situation. Case (1) allows for tracks where resolution or noise hits distort the track away from the IP. Cases (3) and (4) accept events with an extra track produced by an accidental coincidence of noise hits, as well as events with photon conversions into an asymmetric e^+e^- pair. Case (5) accepts events where a companion track is generated by cross talk induced by the signals of a real track. In events satisfying cases (3) or (4), the third track was ignored in further analysis; in events satisfying case (5), only the higher-momentum track of the track pair with $|\Delta\phi|<5°$ was kept.

Because of the differences in energy resolutions and trigger elements between the SC and the end-cap (EC) calorimeters, and the presence of uninstrumented regions between the EC calorimeter modules, it is convenient to divide the detector into two regions: region I: Both CD tracks have $|\cos\theta|<0.80$; region II: any CD track has $|\cos\theta|\geq 0.80$. The following cuts were applied to the two-prong candidates: (1) The noncollinearity angle of the CD tracks must be less than 10°; (2) in region I, the total energy observed in all calorimeters must be greater than $\frac{1}{2}E_{\mathrm{c.m.}}$; (3) in region II, the ratio of the energy ob-

served in the electromagnetic shower calorimeters (E_{SC}) to the energy observed in all calorimeters (E) must satisfy $E_{SC}/E > 0.70$.

Cut (1) rejects $e^+e^- \to e^+e^-e^+e^-$ events, which have predominantly noncollinear tracks. Cut (2) rejects $e^+e^- \to e^+e^-e^+e^-, \mu^+\mu^-, \tau^+\tau^-$ events, which have predominantly low-energy deposition. Cut (3) rejects $e^+e^- \to \mu^+\mu^-$ and $\tau^+\tau^-$ by requiring the energy deposition to be consistent with that of electromagnetic showers.

IV. EFFICIENCY AND BACKGROUND CORRECTIONS

The measured angular distribution must be corrected for detector effects and backgrounds. In addition, the theoretical calculation of the predicted cross section must incorporate higher-order effects. The calculation of these corrections to the accuracy needed to match the small statistical errors of the data is quite difficult; in particular, calculating the corrections using only the full detector simulation[8] is impossible given a reasonable amount of computer time.

Several methods were used to determine the corrections: the study of distributions from the data themselves; the study of Monte Carlo electron-positron pairs with full detector simulation; and the study of events from the Berends and Kleiss[9] (BK) event generator for $e^+e^- \to e^+e^-(\gamma)$, with CD angular resolutions simulated by a simplified Gaussian-approximation Monte Carlo simulation. The BK program, which incorporates a consistent calculation up to order α^3, is the most complete one available in a form useful for experimental corrections.

A. Efficiencies

The MAC trigger is highly efficient for Bhabha-scattering events. Most events were accepted by both the energy and the scintillator triggers. The energy trigger has a high efficiency in region I, since the Bhabha electrons deposit an amount of energy in the calorimeters which is far above the discriminator threshold. The scintillator trigger has a relatively low efficiency in region I, due to the fact that the counters are placed after the SC calorimeter, which has a thickness varying from 14 radiation lengths at normal incidence to 23 radiation lengths near the SC-EC transition region. Nevertheless, the scintillator trigger provides a moderately efficient backup trigger. The situation is reversed in region II, where the energy-trigger efficiency is affected by the dead spaces in the EC but the scintillation-counter efficiency is very high because the counters are placed 8 radiation lengths deep, which is near the depth of largest energy deposition and lateral spread for a 14.5-GeV electromagnetic shower ($\simeq$6.5 radiation lengths).

Table I shows the probability of a scintillator trigger (P_{ST}) for events satisfying the energy trigger, and the probability of an energy trigger (P_{ET}) for events satisfying the scintillator trigger, both as a function of $|\cos\theta|$. The overall trigger efficiency (ϵ_T) derived from these probabilities does not show any significant dependence on $|\cos\theta|$ and has an average value of 0.9990 ± 0.0005.

Dead spaces between the calorimeter modules caused some events to have anomalously low detected energy; these events were lost when energy cuts were applied. In order to study this inefficiency, the azimuthal-angle distributions of the data for the different $|\cos\theta|$ bins were examined. These distributions were found to be flat with small dips at the known positions of the dead spaces. From these distributions the efficiency of the energy cut (ϵ_ϕ) was estimated to have the values listed in Table I. The average efficiency in region I was found to be 0.980 with a standard deviation of 0.004. A study of $e^+e^- \to \gamma\gamma$ events, where a much lower-energy cut was applied, predicted an efficiency of 0.975 ± 0.002, in good agreement with the value above. An overall systematic uncertainty of 0.5% was assigned to ϵ_ϕ.

As was previously mentioned, the two-prong criteria for the CD were designed to be highly efficient. An independent check of the efficiency of this criteria was made with data from the reaction $e^+e^- \to \mu^+\mu^-$. Events were selected that have two tracks reconstructed in the MAC muon spectrometer[10] with the following properties: noncollinearity angle less than 10°; momentum of both tracks greater than 4 GeV; the extrapolation of the tracks must point to a scintillation counter hit; and time-of-flight information consistent with a $\mu^+\mu^-$ hypothesis. Such events would be expected also to satisfy the CD two-prong criteria. The efficiency was measured to be $\epsilon_{CD} = 0.995 \pm 0.0005$ (statistical error only), with no significant angular dependence, in good agreement with the value of 0.996 ± 0.001 predicted by the detector simulation. An overall systematic error of 1.0% was assigned to ϵ_{CD}. This uncertainty was due to two sources: The

TABLE I. Summary of corrections to the $e^+e^- \to e^+e^-$ data, as described in the text.

$\lvert\cos\theta\rvert$	P_{ET}	P_{ST}	ϵ_T	ϵ_ϕ	f_b	$1+\delta(\lvert\cos\theta\rvert)$
0.05	0.9990	0.7071	0.9997±0.0001	0.977±0.002	0.994	0.945±0.005
0.15	0.9991	0.6947	0.9997±0.0001	0.983±0.002	0.995	0.950±0.005
0.25	0.9987	0.6502	0.9996±0.0001	0.980±0.002	0.995	0.958±0.005
0.35	0.9988	0.5708	0.9995±0.0001	0.982±0.002	0.997	0.961±0.005
0.45	0.9985	0.4598	0.9992±0.0002	0.981±0.001	0.998	0.966±0.005
0.55	0.9986	0.3155	0.9991±0.0002	0.984±0.001	0.998	0.992±0.005
0.65	0.9993	0.1330	0.9994±0.0002	0.984±0.001	0.998	1.015±0.005
0.75	0.9983	0.1714	0.9986±0.0002	0.977±0.001	0.996	1.054±0.005
0.85	0.9908	0.9380	0.9994±0.0001	0.991±0.0002	0.997	1.166±0.008

Monte Carlo simulation of the CD did not reproduce exactly the frequency distribution at which the CD tracking criteria were satisfied in the data, and the behavior of muons traversing the beam pipe and central drift chamber is slightly different from that of electrons, due to the difference in their masses.

B. Backgrounds

Bhabha scattering is the dominant process in e^+e^- collisions by a large factor; therefore, backgrounds from other processes are inherently small. The two largest sources of background are the reactions $e^+e^- \to \tau^+\tau^-$ and $e^+e^- \to e^+e^-e^+e^-$. In order to study these backgrounds, Monte Carlo events were generated for both reactions,[11,12] propagated through the detector simulation and processed through the analysis programs. The estimated backgrounds are very small, as can be seen from the purity fractions f_b listed in Table I, where $f_b = S/(S+B)$, with S representing the true signal and B the background. The background is dominated by τ pair production at large scattering angles and by the two-photon process at small scattering angles.

C. Radiative corrections

Radiative corrections are important at high energies, since the probability of energetic initial- or final-state radiation is quite high. The calculation of these corrections was performed using the BK event generator for $e^+e^- \to e^+e^-(\gamma)$, which incorporates a complete calculation to order α^3, including bremsstrahlung, vertex, and vacuum-polarization corrections. The contributions to the cross section of diagrams with order α^4 and higher are expected to be negligible at our energies.[13] The four-vectors generated for the e^+ and e^- were smeared in ϕ and θ using Gaussian approximations for the CD resolution functions. The widths of the Gaussians (as a function of $|\cos\theta|$) were obtained by analyzing e^+e^- events processed through the detector simulation program.

Since the angular cross section varies more than 1 order of magnitude over the acceptance of the detector, the calculation must be performed in several overlapping pieces, each of which has different restrictions on the range of $|\cos\theta|$ over which the events are generated. The radiative correction function $\delta(|\cos\theta|)$ is defined as

$$\frac{d\sigma_{\alpha^3}}{d\Omega} = \frac{d\sigma_{\alpha^2}}{d\Omega}[1+\delta(|\cos\theta|)]$$

and it is listed, for our particular selection criteria, in Table I. The statistical uncertainty in the function value is about 0.5% for all values of $|\cos\theta|$. The systematic error introduced by the uncertainty in the overall normalization for each Monte Carlo run is less than 0.1%.

The sensitivity of the radiative corrections to the selection criteria has been studied by varying the values of the cuts. Only the region with $|\cos\theta| > 0.8$ was found to be sensitive, leading to an additional systematic uncertainty in the overall normalization of 1%.

V. THE $e^+e^- \to e^+e^-$ CROSS SECTION

The angular cross section was obtained from the expression

$$\frac{d\sigma}{d\Omega} = \frac{1}{2\pi\Delta x}\frac{f_b(x)N(x)}{\epsilon(x)[1+\delta(x)]\int \mathscr{L}\,dt},$$

where $x = |\cos\theta|$, $f_b(x)$ is the purity fraction, $N(x)$ is the number of events in each x bin, obtained by giving each track a weight of $\frac{1}{2}$, $\epsilon(x)$ is the overall efficiency, $[1+\delta(x)]$ is the radiative correction function, $2\pi\Delta x$ is a solid angle factor, and $\int \mathscr{L}\,dt = (127.6 \pm 1.1 \pm 1.6)$ pb^{-1} is the integrated luminosity obtained from the measured cross section of the process $e^+e^- \to \gamma\gamma$, presented in the preceding paper.[6] The overall efficiency is the product of the efficiencies described earlier, namely, $\epsilon(x) = \epsilon_T(x)\epsilon_\phi(x)\epsilon_{CD}$.

The resulting differential cross section, illustrated in Fig. 1(a) and listed in Table II, can be compared directly to the predictions of lowest-order QED or electroweak theory. The overall normalization agrees well with the predictions of QED or the electroweak model for a wide

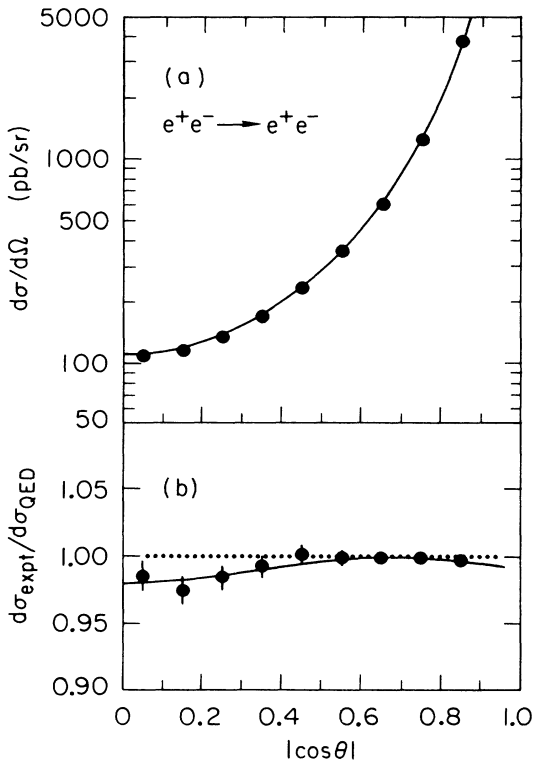

FIG. 1. (a) The experimentally observed $e^+e^- \to e^+e^-$ differential cross section (points) compared to the prediction of electroweak theory (solid curve). The uncertainty on each point is smaller than the dot representing the measurement. (b) The ratio of the observed cross section to that predicted by QED (points with error bars). The dotted line is the prediction of QED and the solid curve is the prediction of electroweak theory, as described in the text.

TABLE II. Summary of the observed $e^+e^-\to e^+e^-$ cross section and errors.

$\lvert\cos\theta\rvert$	$d\sigma_{\alpha^2}/d\Omega$ (pb/sr)	Data events	$d\sigma_{\text{expt}}/d\Omega$ (pb/sr)	Statistical error	Systematic error	Total error	% error
0.05	112.0	8076	107.9	1.2	0.7	1.4	1.3
0.15	120.5	8652	115.0	1.2	0.8	1.5	1.3
0.25	139.8	10203	134.5	1.3	0.9	1.6	1.2
0.35	175.2	12965	170.3	1.5	1.1	1.9	1.1
0.45	239.0	17967	234.7	1.8	1.6	2.4	1.0
0.55	360.0	27686	352.2	2.1	2.4	3.2	0.9
0.65	615.9	48412	601.9	2.7	4.0	4.9	0.8
0.75	1277.2	103480	1239.9	3.8	8.3	9.1	0.7
0.85	3821.1	346826	3755.4	6.4	25.1	25.8	0.7

range of parameters (since the normalization is mostly sensitive to the number of events at small angles, which is nearly independent of electroweak effects). The ratio of the observed total cross section to the QED prediction is

$$\frac{\sigma_{\text{expt}}}{\sigma_{\text{QED}}}=0.99\pm0.001\pm0.015\pm0.015\ ,$$

where the first error is statistical, the second is the systematic error in the number of $e^+e^-\to e^+e^-$ events due to systematic uncertainties in the efficiencies and radiative corrections, and the third error is the systematic error due to the uncertainty in the luminosity measured with the process $e^+e^-\to\gamma\gamma$.

VI. TESTS OF ELECTROWEAK THEORY

The prediction of lowest-order QED for the Bhabha-scattering angular distribution is[14]

$$\frac{d\sigma_{\alpha^2}}{d\Omega}=\frac{\alpha^2}{2s}\left[\frac{u^2+s^2}{t^2}+\frac{2u^2}{ts}+\frac{u^2+t^2}{s^2}\right]=\frac{\alpha^2}{4s}\left[\frac{3+\cos^2\theta}{1-\cos\theta}\right]^2,$$

where (s,t,u) are the standard Mandelstam variables,[15] given by $s=E_{\text{c.m.}}{}^2$, $t=-\frac{1}{2}E_{\text{c.m.}}{}^2(1-\cos\theta)$ and $u=-\frac{1}{2}E_{\text{c.m.}}{}^2(1+\cos\theta)$ in the center-of-mass frame with the approximation $m_e/s\to0$ (m_e is the mass of the electron). Since the cross section varies by more than 1 order of magnitude from $\lvert\cos\theta\rvert=0.0$–$0.9$, it is better to present the data as the ratio $d\sigma_{\text{expt}}/d\sigma_{\text{QED}}$, which can be displayed on a linear scale as shown in Fig. 1(b). The data exhibit a systematic dip as $\lvert\cos\theta\rvert\to0$ and are not well described by the pure QED prediction [dotted line in Fig. 1(b)].

The electroweak theory predicts a deviation from pure QED, due to the diagrams where a Z^0 boson is exchanged. The electroweak differential cross section for $e^+e^-\to e^+e^-$ is given by the expression[3]

$$\frac{4s}{\alpha^2}\frac{d\sigma}{d\Omega}=\left[\frac{3+x^2}{1-x}\right]^2+2v^2(3+x^2)\frac{(3+x)Q-x(1-x)R}{(1-x)^2}-2a^2\frac{(7+4x+x^2)Q+(1+3x^2)R}{(1-x)}$$
$$+(v^2-a^2)^2\frac{8\lvert Q\rvert^2}{(1-x)^2}+\tfrac{1}{2}(v^2-a^2)^2\lvert R\rvert^2(1-x)^2+\tfrac{1}{2}F_1F_2(1+x)^2\ ,$$

where

$$v=2g_V^e,\quad a=2g_A^e,\quad x=\cos\theta\ ,$$
$$s=E_{\text{c.m.}}{}^2,\quad q^2=-\tfrac{1}{2}s(1-x)\ ,$$
$$Q=\tfrac{1}{4}\text{Re}[\chi(q^2)],\quad R=\tfrac{1}{4}\text{Re}[\chi(s)]\ ,$$
$$F_1=[2Q/(1-x)-R]^2,\quad F_2=v^4+6v^2a^2+a^4\ .$$

The function $\chi(s)$ is the propagator for the Z^0 boson, given by

$$\chi(s)=\frac{1}{2\pi\alpha}\frac{G_F}{\sqrt{2}}\rho m_Z\left[\frac{s}{s-m_Z{}^2+im_Z\Gamma_Z}\right]=\frac{1}{\sin^2\theta_W\cos^2\theta_W(1-\Delta)}\left[\frac{s}{s-m_Z{}^2+im_Z\Gamma_Z}\right],$$

where G_F is the Fermi weak-interaction constant and ρ is a parameter that sets the ratio of the strengths of the charged and neutral weak currents. The quantities m_Z and Γ_Z are the mass and width of the Z^0 boson, respectively. The second form of the expression for $\chi(s)$ is obtained from the Glashow-Salam-Weinberg (GSW) model,[1] where ρ and m_Z are assumed to be given in terms of the Weinberg angle (θ_W) and the mass of the $W^\pm$ bosons (m_W) through the expressions

$$\rho=\frac{m_W{}^2}{m_Z{}^2\cos^2\theta_W}\ ,$$
$$m_W{}^2=\frac{\pi\alpha}{\sqrt{2}G_F}\frac{1}{\sin^2\theta_W(1-\Delta)}\ .$$

The factor of $(1-\Delta)$, with $\Delta=0.07$, arises from the self-

energy correction to the Z^0 propagator.[16] In the GSW model, where $\rho=1$, $g_A^e=-\frac{1}{2}$ and $g_V^e=-\frac{1}{2}(1-4\sin^2\theta_W)$, the world-average value of $\sin^2\theta_W=0.22$ leads to $m_Z=93$ GeV and $g_V^e=-0.06$.

The experimentally measured differential cross section was fitted to the electroweak prediction by minimizing a χ^2 derived from a likelihood function which treats separately the shape of the angular distribution and the overall normalization, and includes all systematic errors.[17] The electroweak couplings were allowed to vary, with constant values $\sin^2\theta_W=0.22$ and $m_Z=93$ GeV used to calculate $\chi(s)$, giving the values

$$(g_A^e)^2=0.33\pm0.24,\quad (g_V^e)^2=0.09\pm0.14$$

(with $\chi^2/\mathrm{DF}=3.2/7$). The result of the fit is displayed as the solid line in Fig. 1(b); as can be seen, the data are described extremely well by the electroweak function. The uncertainties in the values of the weak couplings quoted above include all correlations and were obtained, in the standard way, by finding the value of parameter x_j for which the χ^2 changed by one unit after minimization with respect to all other parameters (x_i, $i\neq j$) (Ref. 18). This is important, since $(g_A^e)^2$ and $(g_V^e)^2$ are strongly correlated with each other (correlation coefficient $=0.9$) as well as with the efficiencies and the integrated luminosity.

The results may be presented more completely as the 1σ and 2σ covariance ellipses in $(g_A^e)^2$-$(g_V^e)^2$ space, as shown in Fig. 2. As can be seen in the figure, the solution corresponding to pure QED ($g_A^e=g_V^e=0$) lies near the 2σ contour, whereas the solution corresponding to the nominal GSW couplings [$(g_A^e)^2=0.25$, $(g_V^e)^2\simeq0$] lies on the 0.8σ contour.

A more rigorous statistical treatment can be accomplished by using the likelihood ratio test.[19] The likelihood ratio Q is simply defined as

$$Q=\frac{\text{likelihood of hypothesis 1}}{\text{likelihood of hypothesis 2}}\ .$$

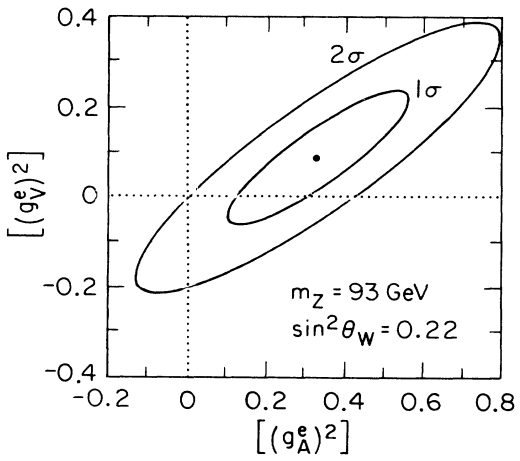

FIG. 2. Covariance ellipses in $(g_A^e)^2$-$(g_V^e)^2$ space, as described in the text.

Under rather general assumptions, the quantity $-2\ln Q$ is expected to have a χ^2 probability distribution, allowing the assignment of a confidence level to one hypothesis over another, without use of the Gaussian distribution assumptions needed to obtain the covariance ellipse. The two hypotheses compared are QED and the GSW model with $\sin^2\theta_W=0.22$. The logarithm-likelihood ratio obtained, $-2\ln Q=3.5$, corresponds to a confidence level of 94% for GSW being the preferred hypothesis.

Additional fits were performed to extract various parameters under more restrictive assumptions. The value

$$(g_V^e)^2=0.05\pm0.06$$

was obtained under the further assumption $(g_A^e)^2=0.25$. This assumed value is supported by experimental data on $e^+e^-\to\mu^+\mu^-,\tau^+\tau^-$ (Ref. 20) (assuming lepton universality) and neutrino scattering. In the context of the GSW model, where m_Z is a function of $\sin^2\theta_W$, the value

$$\sin^2\theta_W=0.24^{+0.18}_{-0.17}$$

was obtained, corresponding to $0.01<\sin^2\theta_W<0.55$ at the 95% confidence level. It should be noted that the χ^2 function is rather badly behaved in this parametrization, so that artificially small errors can result if the fit to the data prefers negative values of $(g_V^e)^2$.

High-precision data on the process $e^+e^-\to e^+e^-$ is limited;[21–25] the most recently published values for the weak couplings extracted by the HRS (Ref. 21) group at PEP and the PLUTO (Ref. 22) and TASSO (Ref. 23) groups at the DESY storage ring PETRA are compared to the MAC values in Table III. Comparison of the individual parameters is difficult because of the high correlation between $(g_A^e)^2$ and $(g_V^e)^2$. All experiments are consistent with the expectations from the GSW model. The MAC result, which includes a full account of systematic errors and a rigorous analysis of the statistical significance of the measurements, indicates the presence of electroweak effects at the 95% confidence level.

The measurement of electroweak effects in Bhabha scattering can be combined with measurements of the reaction $\bar{\nu}_e e^-\to\bar{\nu}_e e^-$ to obtain an unambiguous precision measurement of the electroweak coupling constants of the electron. The two reactions used involve only the leptons which form the first weak-isospin doublet; therefore, the couplings may be determined without assumptions about universality among lepton families or complications from hadronic interactions. The elastic scattering cross section for $\bar{\nu}_e e^-\to\bar{\nu}_e e^-$ is measured with $\bar{\nu}_e$ beams from nuclear

TABLE III. Comparison of electroweak parameters with those of other experiments.

Experiment	$(g_A^e)^2$	$(g_V^e)^2$
MAC	0.33 ± 0.24	0.09 ± 0.14
HRS[a]	0.46 ± 0.14	0.03 ± 0.09
PLUTO[b]	0.39 ± 0.20	0.09 ± 0.12
TASSO[c]	0.01 ± 0.16	-0.15 ± 0.14

[a]Reference 21.
[b]Reference 22.
[c]Reference 23.

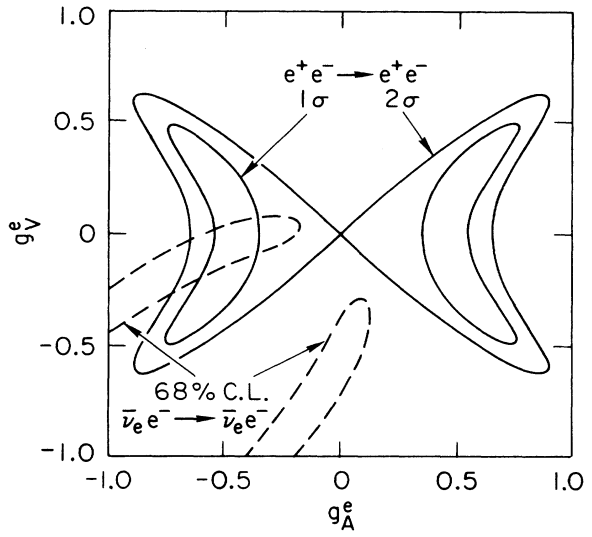

FIG. 3. Contour plots in g_A^e-g_V^e space from $e^+e^- \rightarrow e^+e^-$ and $\bar{\nu}_e e^- \rightarrow \bar{\nu}_e e^-$ measurements, as described in the text.

reactors. The total cross section,[26] in terms of the laboratory antineutrino energy ($E_{\bar{\nu}}$), is given by

$$\sigma(\bar{\nu}_e e^-) = \frac{G_F{}^2 m_e E_{\bar{\nu}}}{2\pi}[(g_V^e - g_A^e)^2 + \tfrac{1}{3}(2 + g_V^e + g_A^e)^2] \ .$$

This expression has linear as well as quadratic dependence on the couplings, as opposed to the $e^+e^- \rightarrow e^+e^-$ cross section, for which the dependence is strictly quadratic. Since the neutrino cross section above depends on two parameters, a measurement of $\sigma(\bar{\nu}_e e^-)$ constrains the parameters to lie along some path in the g_A^e-g_V^e plane; furthermore, from the algebraic symmetry of the formula, the path will have a reflection symmetry about the $g_A^e = g_V^e$ line. This is illustrated in Fig. 3, where the dashed lines represent the 68%-confidence-level contour allowed by the measurements of the $\bar{\nu}_e e^- \rightarrow \bar{\nu}_e e^-$ total cross section.[26] Superimposed as solid-line contours in the figure are the 1σ and 2σ contours of the measurement reported here, obtained by unfolding the covariance ellipse with the assumption that g_A^e and g_V^e are real numbers. These contours have obvious symmetries about the $g_A^e = 0$ and $g_V^e = 0$ lines, since the angular distribution depends quadratically on the couplings. The complementary nature of the measurements is now clearly seen; the combination of the Bhabha- and antineutrino-scattering data selects a unique solution for the electroweak couplings of the electron. A combined fit of both data sets results in

$$g_A^e = -0.48 \pm 0.12, \quad g_V^e = -0.05 \pm 0.09$$

(with $\chi^2/\mathrm{DF} = 4.4/9$), in excellent agreement with the expectations of the GSW model. This value of g_V^e implies $\sin^2\theta_W = 0.23 \pm 0.05$, in good agreement with the world average.

VII. TESTS OF COMPOSITE MODELS OF THE ELECTRON

It has been proposed that the leptons and quarks might in fact be composite objects.[27] Such internal structure leads to additional interactions generated by constituent exchange. Although there is no general consensus on the precise theoretical model describing composite leptons and quarks, it has been pointed out that any such model contains flavor-diagonal, helicity-conserving contact interactions,[28] with a Lagrangian of the form

$$\mathscr{L}_{\psi\psi} = \frac{g^2}{2\Lambda_\pm{}^2}(\eta_{LL}\bar{\psi}_L\gamma_\mu\psi_L\bar{\psi}_L\gamma^\mu\psi_L + \eta_{RR}\bar{\psi}_R\gamma_\mu\psi_R\bar{\psi}_R\gamma^\mu\psi_R + 2\eta_{RL}\bar{\psi}_R\gamma_\mu\psi_R\bar{\psi}_L\gamma^\mu\psi_L) \ ,$$

where the subscripts L and R refer to left- and right-handed helicities, g is an effective coupling constant for the interaction that binds the composites into fermions, and $\Lambda_\pm$ is the characteristic energy scale of that interaction. The η_{ij} are used to select the helicity properties of the interaction and the subscript $\pm$ refers to the sign of η_{LL}. The normalization of Ref. 28 was used, where Λ is defined such that $g^2/4\pi = 1$ and the largest $|\eta_{ij}| = 1$.

The modified $e^+e^- \rightarrow e^+e^-$ cross section, obtained by adding the contact interaction to the usual electroweak Lagrangian, can be written as

$$\frac{4s}{\alpha^2}\frac{d\sigma}{d\Omega} = 4A_0 + A_-(1-\cos\theta)^2 + A_+(1+\cos\theta)^2 \ ,$$

where

$$A_0 = \left|\frac{s}{t}\right|^2 \left|1 + \frac{g_R g_L}{e^2}\frac{t}{t_z} + \frac{\eta_{RL}t}{\alpha\Lambda^2}\right|^2 \ ,$$

$$A_- = \left|1 + \frac{g_R g_L}{e^2}\frac{s}{s_z} + \frac{\eta_{RL}s}{\alpha\Lambda^2}\right|^2 \ ,$$

$$A_+ = \frac{1}{2}\left|1 + \frac{s}{t} + \frac{g_R{}^2}{e^2}\left(\frac{s}{s_z} + \frac{s}{t_z}\right) + \frac{\eta_{RR}s}{\alpha\Lambda^2}\right|^2 + \frac{1}{2}\left|1 + \frac{s}{t} + \frac{g_L{}^2}{e^2}\left(\frac{s}{s_z} + \frac{s}{t_z}\right) + \frac{\eta_{LL}s}{\alpha\Lambda^2}\right|^2 \ ,$$

with $s_z = s - m_Z{}^2 + i m_Z\Gamma_Z$, $t_z = t - m_Z{}^2 + i m_Z\Gamma_Z$, $g_R = e\tan\theta_W$, and $g_L = -e\cot 2\theta_W$ (e is the electron charge).

The important observation is that the modified $e^+e^- \rightarrow e^+e^-$ differential cross section given above contains interference terms of order $q^2/\alpha\Lambda^2$ relative to the GSW model contribution. This effect masks the order q^2/Λ^2 effects due to the more traditional propagator form factors,[29] such as those used in the analysis of $e^+e^- \rightarrow \gamma\gamma$.

Fits of the data to the modified cross section (with $\sin^2\theta_W = 0.22$ fixed) were performed for several choices of η_{ij}, as seen in Table IV. All the results are consistent

TABLE IV. Limits on the energy scale for electron substructure from $e^+e^- \to e^+e^-$. Because of the symmetry in the contact interaction Lagrangian, the right-right interaction result is identical to the left-left result.

Interaction	η_{LL}	η_{RL}	η_{RR}	Limit on Λ (TeV)
Left-left	+1	0	0	>1.0
Left-left	−1	0	0	>0.7
Vector	+1	+1	+1	>3.0
Vector	−1	−1	−1	>2.1
Axial vector	+1	+1	−1	>1.8
Axial vector	−1	−1	+1	>2.3

with a null effect and the limits on Λ are in the 1-TeV range. These limits are similar to those obtained by other experiments[21,23] and indicate that electrons are pointlike at least up to energy scales 10 times greater than the electroweak energy scale.

VIII. CONCLUSIONS

A high-precision measurement of the $e^+e^- \to e^+e^-$ differential cross section has been presented. A statistically significant deviation from pure quantum electrodynamics is observed, providing evidence for electroweak interference effects in this reaction. The values obtained for the electroweak couplings of the electron are in good agreement with the expectations from the Glashow-Salam-Weinberg model and previous measurements. This measurement is complementary to $\bar{\nu}_e e^-$ elastic-scattering experiments and the combined results allow an unambiguous determination of the electroweak couplings of the electron. The agreement between the data and the electroweak theory prediction is used to put limits on substructure of the electron up to mass scales on the order of 1 TeV.

ACKNOWLEDGMENTS

We acknowledge the technical assistance of C. T. Pulliam. We also acknowledge the technical assistance of N. Erickson, J. Escalera, M. J. Frankowski, and J. Schroeder and the help of J. Kolonko, M. Richards, and J. Richeson. This work was supported in part by the U.S. Department of Energy under Contracts Nos. DE-AC02-81ER40025 (University of Colorado), DE-AC03-76SF00515 (SLAC), and DE-AC02-76ER00881 (University of Wisconsin); by the National Science Foundation under Contracts No. NSF-PHY82-15133 (University of Houston), NSF-PHY82-15413, NSF-PHY82-15414 (Northeastern University), and NSF-PHY83-08135 (University of Utah); and by the Istituto Nazionale di Fisica Nucleare.

*Present address: Universidad Autónoma de Barcelona, Barcelona, Spain.
†Present address: CERN, Geneva, Switzerland.
‡Joint appointment: Department of Physics and College of Computer Science, Northeastern University, Boston, MA 02115.
§Permanent address: CERN, Geneva, Switzerland.
**Present address: Laboratory for Nuclear Studies, Cornell University, Ithaca, NY 14853.

[1]S. L. Glashow, Nucl. Phys. **22**, 579 (1961); A. Salam, in *Elementary Particle Theory: Relativistic Groups and Analyticity*, (Nobel Symposium No. 8), edited by N. Svartholm (Almqvist and Wiksell, Stockhom, 1968), p. 367; S. Weinberg, Phys. Rev. Lett. **19**, 1264 (1967).
[2]R. Budny, Phys. Lett. **55B**, 227 (1975).
[3]R. Budny, Phys. Lett. **58B**, 338 (1975).
[4]The MAC coordinate system is defined as follows: the z axis follows the positron direction in PEP; the x axis points toward the center of the storage ring; and the y axis points upward. The angle ϕ is the aximuthal angle in the x-y plane and θ is the polar angle with respect to the z axis. The differential solid angle $d\Omega$ is given by $2\pi d(\cos\theta)$.
[5]E. Fernandez *et al.*, Phys. Rev. D **31**, 1537 (1985); B. K. Heltsley, Ph.D. thesis, 1983, University of Wisconsin; W. T. Ford, in Proceedings of the International Conference on Instrumentation for Colliding Beams, edited by W. W. Ash [SLAC Report No. SLAC-250, 1982 (unpublished)].
[6]E. Fernandez *et al.*, preceding paper, Phys. Rev. D **35**, 1 (1987).
[7]B. Gottschalk, Nucl. Instrum. Methods **190**, 67 (1981).
[8]The MAC detector simulation program is a detailed geometrical description of the detector, combined with two radiation transport packages: EGS (electron-gamma-shower code) for electron and photon shower simulation, R. L. Ford and W. R. Nelson, SLAC Report No. SLAC-0210, 1978 (unpublished); and HETC (high-energy-transport code) for hadron showers and muon energy deposition, T. A. Gabriel and B. L. Bishop, Nucl. Instrum. Meth. **155**, 81 (1978).
[9]F. A. Berends and R. Kleiss, Nucl. Phys. **B228**, 537 (1983).
[10]G. P. Goderre, Ph.D. thesis, 1985, Northeastern University Report No. NUB-2687 (unpublished).
[11]F. A. Berends and R. Kleiss, Nucl. Phys. **B177**, 237 (1981).
[12]J. Smith, J. A. M. Vermaseren, and G. Grammer, Jr., Phys. Rev. D **15**, 3280 (1977).
[13]Y. S. Tsai, Report No. SLAC-PUB 3129, 1983 (unpublished).
[14]An excellent introduction to the standard model is given in F. Halzen and A. Martin, *Quarks and Leptons: An Introductory Course in Modern Particle Physics* (Wiley, New York, 1984); also see E. Leader and E. Pedrazzi, *An Introduction to Gauge Theories and the "New Physics"* (Cambridge University, Cambridge, England, 1982).
[15]In a two-body reaction $ab \to cd$ where a,b,c,d are particles described by four-vectors a,b,c,d, the Mandelstam variables are defined as $s=(a+b)^2$, $t=(a-c)^2$, and $u(a-d)^2$.
[16]M. Böhm and W. Hollik, Phys. Lett. **139B**, 213 (1984); R. W. Brown, R. Decker, and E. A. Paschos, Phys. Rev. Lett. **52**, 1192 (1984); W. J. Marciano and A. Sirlin, Phys. Rev. D **29**, 945 (1984).
[17]M. C. Delfino, Ph.D. thesis, 1985, University of Wisconsin Report No. WISC-EX-85/263.
[18]The fitting package MINUIT was used. F. James and M. Roos, Comput. Phys. Commun. **10**, 343 (1975). Also see F. James, CERN Computer Centre Program Library long-write-up supplement D506, 1978 (unpublished).

[19]See one of the standard statistical analysis texts, for example, Stuart L. Meyer, *Data Analysis for Scientists and Engineers* (Wiley, New York, 1975).

[20]See, for instance, E. Fernandez *et al.*, Phys. Rev. Lett. **55**, 1831 (1985); **54**, 1620 (1985).

[21]M. Derrick *et al.*, Phys. Lett. **166B**, 463 (1986); Phys. Rev. D **34**, 3286 (1986).

[22]C. Berger *et al.*, Z. Phys. C **27**, 341 (1985).

[23]M. Althoff *et al.*, Z. Phys. C **22**, 13 (1984).

[24]W. Bartel *et al.*, Z. Phys. C **19**, 197 (1983).

[25]H. J. Behrend *et al.*, Z. Phys. C **16**, 301 (1983).

[26]F. Reines *et al.*, Phys. Rev. Lett. **37**, 315 (1976); F. T. Avignone *et al.*, Phys. Rev. D **16**, 2383 (1977); W. Krenz, Physikalisches Institut, Technische Hochschule Aachen, Germany, Report No. PITHA 82/26, 1982 (unpublished).

[27]For a review of composite models see, for example, M. E. Peskin, in *Proceedings of the 1981 International Symposium on Lepton and Photon Interactions at High Energy,* Bonn, edited by W. Pfeil, (Physikalisches Institut, Universität Bonn, 1981), p. 880.

[28]E. J. Eichten, K. D. Lane, and M. E. Peskin, Phys. Rev. Lett. **50**, 811 (1983).

[29]N. M. Kroll, Nuovo Cimento **A45**, 65 (1966); A. Litke, Ph.D. thesis, Harvard University, 1970.